Radiation Physics and Chemistry 181 (2021) 109327

Contents lists available at ScienceDirect

Radiation Physics and Chemistry

journal homepage: www.elsevier.com/locate/radphyschem

Calculation of dose point kernel values for monoenergetic electrons and beta emitting radionuclides: Intercomparison of Monte Carlo codes

Bruno Melo Mendes [a,*], Paula Cristina Guimarães Antunes [b], Isabela Soares Lopes Branco [b], Eduardo do Nascimento [c], Baljeet Seniwal [d], Telma Cristina Ferreira Fonseca [d], Helio Yoriyaz [b]

[a] Centro de Desenvolvimento da Tecnologia Nuclear, CDTN, Av. Presidente Antônio Carlos, 6.627 Campus da UFMG – Pampulha, 31270-901, Belo Horizonte, Minas Gerais, Brazil
[b] Instituto de Pesquisas Energéticas e Nucleares, IPEN, 05508-000, São Paulo, SP, Brazil
[c] Universidade Federal da Bahia, UFBA, Instituto de Humanidades, Artes e Ciências, IHAC, 40170-110, Salvador, BA, Brazil
[d] Departamento de Engenharia Nuclear - Universidade Federal de Minas Gerais, Av. Antônio Carlos, 6.627, Pampulha, 31270-901, Belo Horizonte, MG, Brazil

ARTICLE INFO

Keywords:
Targeted radionuclide therapy
Beta-emitting seeds brachytherapy
Electron DPK
MC code intercomparison

ABSTRACT

Targeted radionuclide therapy (TRT) and beta-emitting seeds brachytherapy (BSBT) exploit the characteristics of energy deposited by beta-emitting radionuclides. Monte Carlo (MC) modelling of electron transport is crucial for calculations of absorbed dose for TRT and BSBT. However, computer codes capable of providing consistent results are still limited. Since experimental validations show several difficulties, the estimation of electron dose point kernel (DPK) is often used to verify the accuracy of different MC codes. In this work, we compared DPK calculations for various point, isotropic and monoenergetic electron sources and several beta-emitting radioisotopes using the codes MCNP, EGSnrc, PENELOPE and TOPAS with different simulation options. The simulations were performed using latest versions of EGSnrc and Penelope, TOPAS version 3.3.1 and MCNP version 6.1 Monte Carlo codes. In our simulations, the geometrical model consists of a point electron source placed at the center of a water sphere emitting isotropically. The water sphere was divided into 28 shells and the energy deposition was scored within these shells. The radius of the outermost shell was $1.2R_0$, where R_0 is the continuous slowing down approximation (CSDA) range. Five monoenergetic beta sources with energies of 0.05, 0.1, 0.5, 1 and 3 MeV were studied. Six beta-emitting radionuclides were also simulated: Lu-177, Sm-153, Ho-166, Sr-89, I-131 and Y-90. Monoenergetic electron simulations showed large deviations among the codes, larger than 13% depending on the electron energy and the distance from the source. In the cases where beta spectra of radionuclides were simulated, all MC codes showed differences from EGSnrc (used as reference value - RV) less than 3% within r_{E90} range (radius of the sphere in which 90% of the energy of the spectrum electrons would be deposited). TOPAS showed results comparable to EGSnrc and PENELOPE. DPK values for 0.1 MeV monoenergetic electrons, calculated using MCNP6, led to differences higher than ±5% from RV despite our attempts to tune electron transport algorithms and physics parameters.

1. Introduction

Radiation therapies involving the use of beta particle emitting radionuclides have been widely studied and used. Targeted radionuclide therapy (TRT) and beta-emitting seeds brachytherapy (BSBT) are the examples of techniques that take advantage of the characteristic energy deposition of this type of particle (Gudkov et al., 2015; Khorshidi et al., 2015; Passos et al., 2016; Sapienza and Willegaignon, 2019).

TRT uses high affinity carriers to selectively deliver radionuclides to tumor cells (Gudkov et al., 2015; Wheat et al., 2011). Several types of carriers have been used, including: antibodies, antigens, liposomes, carbon nanotubes, aptamers, microspheres, specific molecules and nanoparticles (Gudkov et al., 2015; Jeon, 2019; Li et al., 2017; Sapienza and Willegaignon, 2019; Wang et al., 2020a,b). In some cases, the radionuclide itself has affinity for tumor tissues, for instance the Iodine and the thyroid gland. Among the beta emitters conjugated to tumor-seeking macromolecules are Sr-89, Y-90, I-131, Sm-153, Ho-166 and Lu-177 (Gudkov et al., 2015; Jeon, 2019; Li et al., 2017; Sapienza

* Corresponding author.
E-mail address: bmm@cdtn.br (B.M. Mendes).

https://doi.org/10.1016/j.radphyschem.2020.109327
Received 16 June 2020; Received in revised form 28 October 2020; Accepted 17 December 2020
Available online 24 December 2020

and Willegaignon, 2019; Wheat et al., 2011), covering a range of energy from few keV to 2.28 MeV (ICRP, 2007). Dosimetry is very important in TRT to determine dose deposition within the tumor volume and organs at risk, i.e., treatment planning and follow up. In addition, it has an important role in microdosimetric studies to evaluate the efficiency of a group radionuclide/carrier based on the dose accumulation pattern within the cell (Bousis et al., 2010; Hindorf et al., 2005; 2007; Seniwal et al., 2020a; Syme et al., 2004).

The first reported use of BSBT using seeds produced from biocompatible glass was in the early 2000s (Roberto et al., 2003a, b). This technique is based on the principle of depositing large amounts of energy in the close proximity (few millimeters) of the radiation source by high energy beta particles in comparison to the photon emitters currently used in brachytherapy. Thus, high dose can be deposited within the tumors and healthy tissues can be spared. Initially, the use of Sm-153 was proposed (Roberto et al., 2003b). Since then, the use of different high energy beta emitters such as Pr-142, Y-90, Re-188, Ho-166 and Sr-89, have been evaluated (Anjomrouz et al., 2016; Calandrino et al., 2007; Hadadi et al., 2013; Hosseini et al., 2013; Jung and Reece, 2008; Khorshidi et al., 2015; Passos et al., 2016). Clinical studies of BSBT have not yet been reported. Dosimetric studies for optimization of seed distribution within tumor volumes and determination of AAPM TG-60 parameters, including reference dose rate, radial dose function and anisotropy function, are required for clinical evaluation of BSBT.

Accurate absorbed dose estimation, which usually is based on Monte Carlo modelling of electron transport, is critical for proper disease control, minimizing the risk of radiation induced deterministic effects for both TRT and BSBT. However, computer codes capable of providing reliable results are still scarce and depend on reliable atomic data and cross-sections. Several electron transport models have been made available along the years by different computer code developers such as Geant4 (Allison et al., 2016), MCNP6 (Goorley et al., 2013), PENELOPE (Baró et al., 1995; Salvat and Fernández-Varea, 2015), TOPAS (Perl et al., 2012), EGSnrc (Kawrakow and Rogers, 2013) and PHITS (Sato et al., 2015).

The MCNP code, up to the MCNPx version, provided the well-known condensed-history method (CHM) for simulating electron transport (Pelowitz, 2011). In MCNP6 the single event (SE) algorithm was also introduced, which considers individual electron collisions (Goorley et al., 2013). Other Monte Carlo (MC) codes can also use SE algorithms. PENELOPE (Salvat and Fernández-Varea, 2015) code can use either CHM or SE, following a predetermined threshold of energy loss defined by the user. EGSnrc (Kawrakow and Rogers, 2013) uses a single scattering mode near the boundaries for accurate simulations. EGSnrc is recognized to be a very stable and electron-transport artifact free code (Reynaert et al., 2002). In 2012, TOPAS MC code (Perl et al., 2012) was launched with applications in medical physics. This code is a wrapper and extension to Geant4, designed with a particular usefulness in proton transport problems considering all secondary particles including neutrons, photons and electrons.

In nuclear medicine, dose point kernel (DPK) is used to verify the accuracy of dosimetric calculations performed using different computer codes. For the calculations, a point, isotropic radioactive source placed at the center of the spherical water phantom and DPK is estimated at different points along the radius of the phantom. Some studies on comparison of electron DPK, calculated using different codes, can be found in literature (Antoni and Bourgois, 2017; Botta et al., 2011; Bousis et al., 2008; Champion et al., 2014; Kyriakou et al., 2019; Maigne et al., 2011; Reynaert et al., 2002). However, these usually compare only two codes (Antoni and Bourgois, 2017; Reynaert et al., 2002). Furthermore, the electron transport models and algorithms used are now outdated (Botta et al., 2011; Champion et al., 2014; Reynaert et al., 2002). In this study, we calculated DPK for various point, isotropic and monoenergetic electron sources and several radioisotopes with potential use in nuclear medicine using the codes: MCNP6, EGSnrc, PENELOPE and TOPAS with different and updated simulation options provided by the updated version of the codes. DPK was calculated in spherical shells composed of water with variable thickness according to electron energy.

2. Materials and methods

2.1. DPK calculation model

The geometrical model consisting of an isotropically emitting, point electron source placed at the center of a water sphere was used. The water sphere was divided into 28 shells and the energy deposition was computed within these shells. The radius of the outermost shell was $1.2R_0$, where R_0 is the continuous slowing down approximation (CSDA) range corresponding to the energy of the monoenergetic electron sources and the maximum energy of the betas emitted by the radionuclides. Five monoenergetic beta sources with energies of 0.05, 0.1, 0.5, 1.0 and 3.0 MeV were studied. Six beta-emitting radionuclides were also investigated: Lu-177, Sm-153, Ho-166, Sr-89, I-131 and Y-90. Fig. 1 shows the model used for the simulations. Table 1 reports the average energy of each radionuclide along with the R_0 and thickness of the shells. The beta emission spectra of the radionuclides was taken from RADAR (RADAR, 2002). Electron fluence within the shells were also obtained for monoenergetic electrons.

Based on the work of Antoni and Bourgois in 2017 (Antoni and Bourgois, 2017), the dose-point kernel is defined as:

$$DPK(r) = D(r).4\pi r^2.\rho.\frac{R_0}{E} \quad (1)$$

where D(r) is the absorbed dose in MeV/g; r is the radial distance in cm; R_0 is the electron CSDA range in cm; ρ is the water density in g/cm^3; E is the electron energy in MeV.

2.2. Monte Carlo codes

2.2.1. MCNP6

Five different routines were used to calculate DPK using MCNP6.1. code version (Goorley et al., 2013). First four routines were based on the default MCNP6 condensed-history algorithm (Landau straggling), varying the EFAC and ESTEP parameters. EFAC controls the spacing of the stopping power energy grid, i.e., the step size. ESTEP controls the number of sub-steps. The sub-step is the level at which the angular deflection and the production of secondary particles are sampled (Goorley et al., 2013).

First CH routine, named as CHdd, used default values for ESTEP (3, for water) and EFAC (0.917). The second routine (CHed) used the default ESTEP value and EFAC increased to 0.99. In the third routine, CHee, EFAC was set to 0.99 and ESTEP parameter was increased according to the methodology described in MCNP5 manual (X-5 Monte

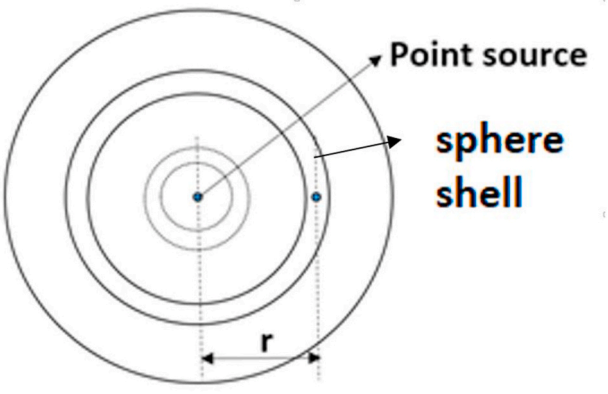

Fig. 1. Geometric model for the simulation. A water sphere composed of multiple shells, varying in radius, where DPK is calculated.

Table 1
Energy, R_0 and, shell thickness for the cases simulated in this work.

Electron Simulated		Avg./Max. Energies (MeV)	R_{CSDA} (cm)	Shell Thickness (cm)
monoenergetic		0.05/0.05	0.0043	0.0000864
		0.1/0.1	0.0143	0.0002862
		0.5/0.5	0.1766	0.0035320
		1/1	0.4367	0.0087340
		3/3	1.5140	0.0302800
Spectrum	Lu-177	0.133/0.498	0.1755	0.003511
	I-131	0.182/0.807	0.3363	0.006725
	Sm-153	0.228/0.808	0.3369	0.006739
	Sr-89	0.584/1.492	0.7048	0.014097
	Ho-166	0.668/1.854	0.8994	0.017987
	Y-90	0.935/2.280	1.1289	0.022577

Carlo Team, 2008) such that an electron should make at least ten sub-steps in any shell it enters. The fourth routine, CHee+, maintained EFAC = 0.99 and the methodology used to calculate ESTEP resulted in values an order of magnitude higher than ones that were obtained for CHee mode. The details of the methodology used to calculate ESTEP and values obtained in each case are presented in the supplementary file.

The fifth routine, named as SE, uses the single event electron transport algorithm. Such an algorithm, completely different from CH electron transport, is based on direct sampling of microscopic data and is designed to improve the accuracy of low-energy electron transport (Hughes, 2014).

For all the five routines, cross sections from ENDF/B-VI release 8 photon/electron-atomic and relaxation data for H and O were used. The energy deposition by electrons within the target volumes (the 28 shells) were scored using Tally *F8. The DPKs were calculated for all five routines (described above). The results of the routine which showed the best match with the reference value (see section 2.3) are plotted in the graphics. The remaining results are included in the supplementary file.

2.2.2. TOPAS

TOPAS (Perl et al., 2012) is a wrapper and extension of the GEANT4 (Allison et al., 2016) Monte Carlo code. It is specialized for simulation of radiotherapy problems. The code allows modeling the LINACs heads and geometry of patients based on tomography (CT) images. It can also incorporate movements, related to the gantry and the geometry of the patient, to perform 4D calculations. Initially, this code was designed for use in proton therapy, but today its application extends to all radiation therapies, and there are also drafts of future versions for including radiobiology parameters and calculations. The simulations were performed using version 3.1.1. of TOPAS, default modular physics list and the energy cut off for electrons and photons was set to 50 eV.

2.2.3. PENELOPE

PENELOPE (Salvat and Fernández-Varea, 2015) MC code allows the transport of electrons, positrons and photons with energy from a few hundred eV to about 1 GeV, in complex geometries and materials of varied chemistry composition. PenEasy (Sempau et al., 2011) is a general-purpose main program for PENELOPE. It includes a set of source models, tallies and variance-reduction techniques that are invoked from a structured code. PENELOPE is a class II code, i.e., positron and electron interactions are simulated using a mixed approach. The event-by-event detailed simulation is performed for hard events and the condensed-history based simulation approach is used for soft interactions. In the present work, the PENELOPE 2018 version associated with PenEasy 2019-09-26 code version was used. The energy cut off for electrons, positrons and photons was set to 50 eV and the simulation parameters that were used for electron and positron transport for condensed-history are C1 = C2 = 0.1, WCC = WCR = 50 and DSMAX = 1030.

2.2.4. EGSnrc

EGSnrc (Kawrakow and Rogers, 2013) is an updated version of the Monte Carlo software Electron Gamma Shower (EGS) for clinical purposes (Fonseca et al., 2020; Seniwal et al., 2019, 2020b). It can simulate the transport of electrons, positrons and photons in the energy range of 1 keV to 1 GeV, within the homogeneous medium. Mixed approach is used to simulate the transport of electrons. Interactions (such as hard bremsstrahlung, hard inelastic collisions, and annihilation) with energy losses greater than the threshold are treated by conventional random sampling. Whereas, sub-threshold interactions such as soft bremsstrahlung emission, soft inelastic collision and elastic scattering are subjected to grouping (Kawrakow and Rogers, 2013). To accurately simulate the transport of electrons in heterogeneous medium or near the interfaces the boundary crossing algorithm (BCA) is used. In this work, the default EXACT algorithm was used as BCA and skin depth for BCA was set to 3. This algorithm activates single scattering (SS) mode to simulate the transport of electrons while crossing the boundaries. The distance from the boundary at which the SS mode is activated is resolved by the 'Skin depth for BCA' parameter. The energy cut off for electron transport was set to 1 keV.

2.3. Code comparison and data analysis

The DPK curves obtained with the EGSnrc MC code were considered as reference values (RV) in order to facilitate the comparison among the codes. A gray area comprising ±3% interval of the EGSnrc curves was included in each graphic.

Simulation relative errors in the outermost shells could be higher than 3%. Thus, the comparisons were restricted from DPK values in the 0–0.9R_0 range in the monoenergetic cases. For radionuclide spectra cases, we compared the DPK data up to r_{E90} value, which corresponds to the radius of the sphere in which 90% of the energy of the spectrum electrons would be deposited.

3. Results and discussion

DPK curves obtained for monoenergetic, point and isotropic electron sources with energy 0.05, 0.1, 0.5, 1 and 3 MeV are shown in Fig. 2. The comparison of the codes was restricted to the DPK values in the 0.9R_0 range (see section 2.3).

PENELOPE data was found in the best agreement with the EGSnrc DPK values (RV). For all points lower than 0.65 R_0, the differences are within ±3% range for all electron energies. TOPAS code also showed a good agreement with RV for 0.1–1.0 MeV electrons. However, TOPAS DPK values for 0.05 MeV and 3.0 MeV electrons showed a greater number of points out of the ±3% range. All codes agree with RV within ±5%, except MCNP6 for 0.1 MeV electrons and TOPAS for 3.0 MeV electrons.

The results obtained with MCNP6 code varied considerably depending on the simulation parameters (as can be seen in supplementary file). SE routine matches very well with the RV (within ±5%) for 0.05 MeV electrons, but for higher energies such as 0.1, 0.5, 1.0 and 3.0 MeV, the discrepancies increase with increase in the source energy (>± 10%; > ± 50%; > ± 90%; > ± 130%; respectively). This behavior was also reported by Antoni and Bourgois (Antoni and Bourgois, 2017) and Poskus (Poškus, 2016). According to Poskus (2016) these discrepancies are caused by the lack of data for angular distribution of elastic scattering in the ENBF/B library. In this case, the linear interpolation of the angular distribution table could cause overestimation of electron backscattering process resulting in a backward shift of the DPK curve.

MCNP6 DPK results obtained using the condensed-history method (CHM) algorithm showed good agreement with EGSnrc, TOPAS and PENELOPE for 0.5, 1.0 and 3.0 MeV monoenergetic electron energies. All differences were less than ±7%, ±6% and ±5% for these energies,

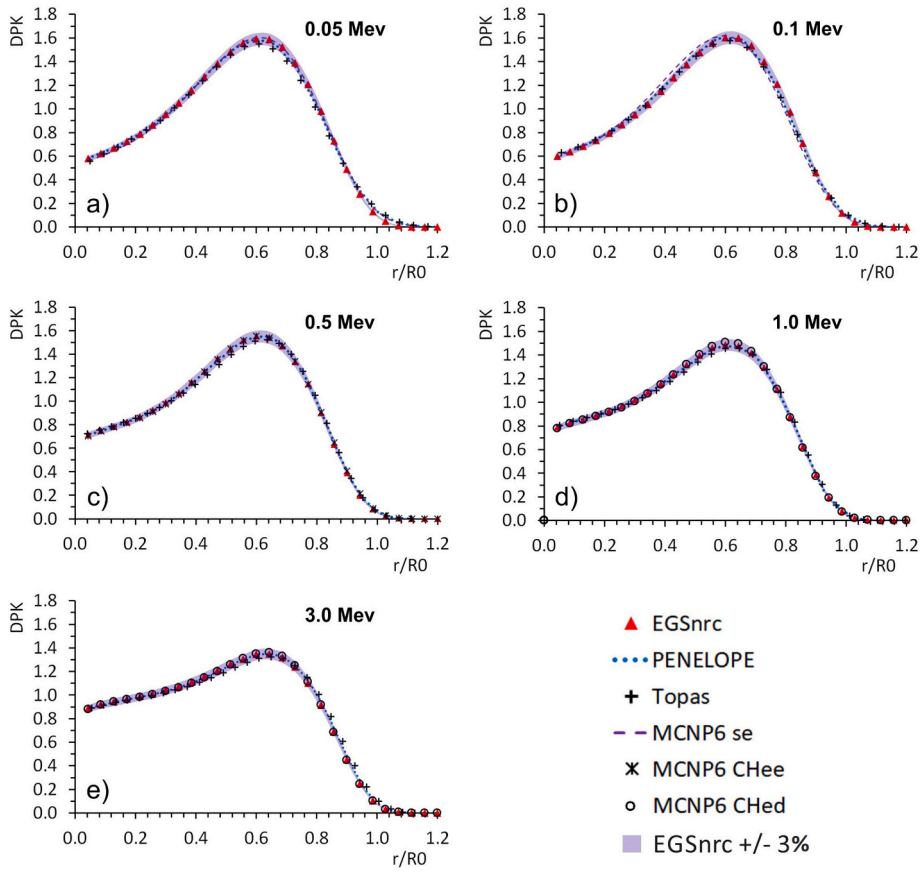

Fig. 2. DPK curves for monoenergetic electron point sources of: a) 0.05, b) 0.1; c) 0.5; d) 1 and e) 3 MeV. The gray area comprises ±3% of the EGSnrc curves.

respectively, except for 3.0 MeV using CHee+ (>20%). Values closer to RV were obtained with CHee routine for 0.5 MeV (4.0% to -1.4%). For 1.0 Mev and 3.0 MeV electrons, CHed routine obtained values closer to RV: (1. 5% to -2.0%) and (1.1% to -1.1%) respectively. For lower energies (such as 0.05 and 0.1 MeV), CH algorithm diverges considerably near the DPK peak (as shown in the supplementary file).

Considering only the CH routines, the increase of ESTEP values and EFAC resulted in DPK closer to RV for 0.05 MeV (CHee), 0.1 MeV (CHee+) and 0.5 MeV (CHee or CHee+). Although, for the two first electron energies, the Single-Event algorithm is preferable. Increasing ESTEP and EFAC for 1.0 MeV and 3.0 MeV electrons did not improve the results and considerably increased the computational time. In this regard, the CHdd mode had the lowest computational times per particle history. CHee and CHee + had, on average, computational times approximately 12x and 85x higher than CHdd, respectively, as can be seen in the supplementary file.

Still about MCNP6, none of the MCNP routines for electron transport, tested for the geometry proposed in this work, show results within ±5% of RV for 0.1 MeV monoenergetic electrons. The SE algorithm presented DPK results closer to the RV than CH algorithms. However, many points were left out of the EGSnrc ±3% range (Fig. 2b). Thus it is important to tune of the electron transport parameters for 0.1 MeV monoenergetic electrons. In fact, for 0.1 MeV electrons, we tested three more routines keeping default value for EFAC and ESTEP parameter was varied. However, the attempts to tune the electrons transport parameters failed to obtain DPK values closer to RV than SE routine. Details of the methodology and results of these tests are included in the supplementary file. The effect of change in the energy cutoff value was also analyzed for the SE algorithm. The results (also added to the supplementary file) show that only electrons with energy below 20 keV could show some improvement with the lowering of cutoff value.

Discrepancies in the DPK curves found here can be better understood by analyzing the corresponding electron fluence for each case. Fig. 3a to e presents the electron fluence curves obtained for the monoenergetic electron point sources with the different codes and methods used.

The fluence curves obtained with MCNP6 (CHed and CHee+) and PENELOPE agreed well with RV along the entire radius of the spherical phantom. In general, the fluence curves obtained with EGSnrc, MCNP6 and PENELOPE showed faster drops than those obtained with TOPAS. Indeed, TOPAS fluence results demonstrated good agreement with other MC codes along the radius of the sphere, up to a certain point of the CSDA range (such as 0.8–1.0 R_0) for all source energies. An increase in deviation is observed with an increase in the electron energy. For 3 MeV electrons, the fluence curve starts diverging at 0.8 R_0. It should be noted that for TOPAS the energy cutoff of 50 eV was used and 3.0 MeV is the only monoenergetic electron case where TOPAS showed a difference higher than ±5% from the RV in the 0.9 R_0 range. TOPAS is a wrapper of Geant4 and it also includes Geant4-DNA facilities as well. So, one possible reason for this deviation can be that TOPAS performed detailed calculations using track structure facilities of Geant4-DNA. Whereas, other MC codes, MCNP6, EGSnrc and PENELOPE are condensed history based code and showed sharp drop in the fluence curves. Also, TOPAS can use a great number of physics constructors options, provided by GEANT4 toolkit, to gather the list of physics processes, particles and physics models desired for the simulation (TOPAS MC, 2016). Thus, fluence output can be tuned, especially for 3.0 MeV electrons, using different physics constructors.

The results calculated by MCNP6 using SE mode showed increasing discrepant values for 0.5 MeV, 1.0 MeV and 3.0 MeV energies. The fluence curves start diverging at 0.8, 0.6 and 0.1 of the CSDA range, for 0.5 MeV, 1 MeV and 3 MeV electrons respectively. The faster drop in the MCNP6 SE fluence results may be responsible for the DPK curve shift to the left, confirming the overestimation of electron backscattering, which is evidenced in SE mode.

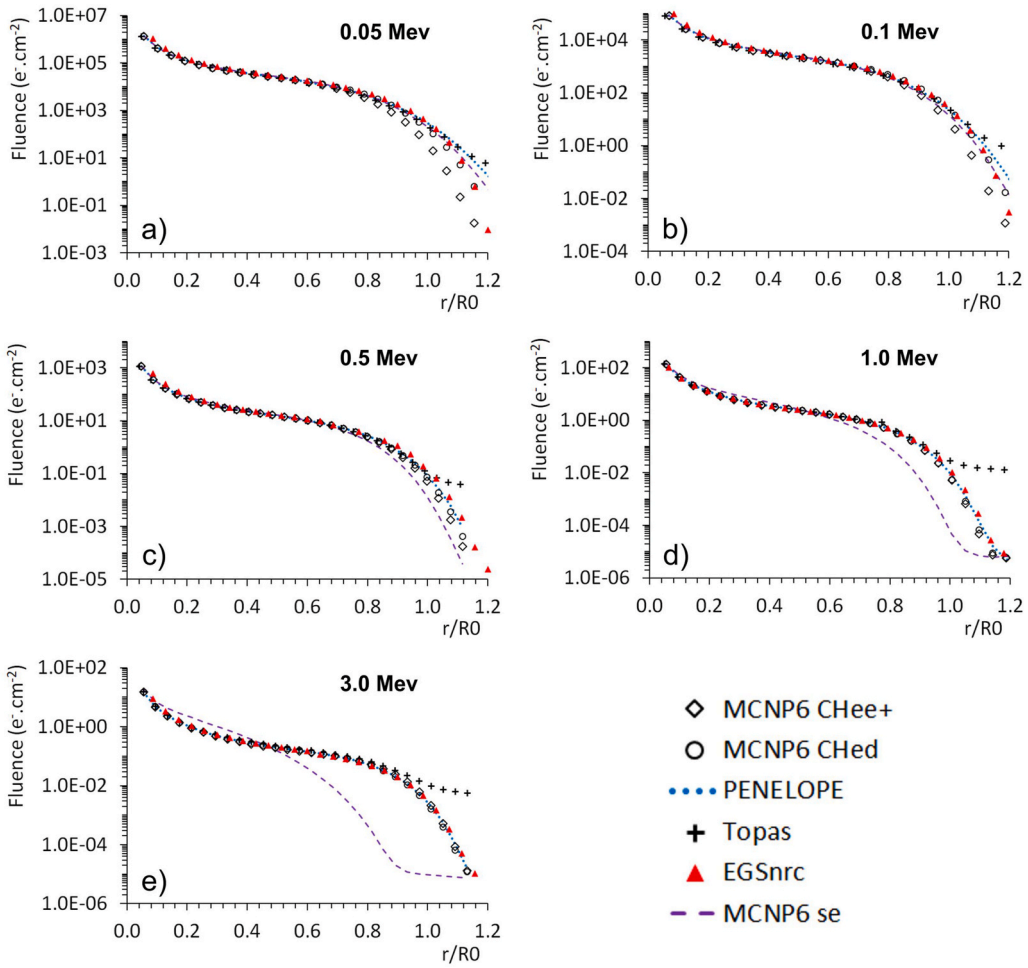

Fig. 3. Fluence curves for monoenergetic electron point sources of: a) 0.05 MeV; b) 0.1 MeV; c) 0.5 MeV; d) 1 MeV; and e) 3 MeV.

The DPK curves obtained for Lu-177, I-131, Sm-153, Sr-89, Ho-166 and Y-90 are presented in Fig. 4. Lu-177, I-131 and Sm-153 are the radionuclides with lowest average energies (0.133 MeV, 0.182 MeV and 0.228 MeV, respectively). Good agreement between all MC codes was observed for the obtained DPK curves, including MCNP6 CH and SE routines. No MC code showed differences greater than 5% in comparison to the reference values obtained for EGSnrc. Results obtained from TOPAS, PENELOPE and MCNP6 routines CHdd and CHee+ were within ±3% deviation, in the r_{E90} range, compared to the EGSnrc curves. Chdd routine showed the best MCNP6 correlation with RV (differences < ± 2%).

Sr-89, Ho-166 and Y-90 are the radionuclides with highest mean energy (0.584 MeV, 0.668 MeV and 0.935 MeV, respectively). All codes, except MCNP6 CHee+ and SE routine, presented discrepancies lower than 5% with respect to EGSnrc reference values. The DPK curves computed using MCNP6 CHdd, CHed, CHee, TOPAS and Penelope were within ±3% of the EGSnrc curves, for these three radionuclides in the r_{E90} range. The best correlation with RV (differences < ± 1%) for MCNP6 was observed with CHed routine. Huge discrepancies (even higher than 70%) were observed for the results obtained with MCNP6 SE algorithm and it should not be used with higher energy radionuclides.

The increase in ESTEP value (CHee and CHee+) did not calculate the DPK values closer to RV for any radionuclide spectra simulations. The only improvement in DPK calculations observed was for 0.5 keV monoenergetic electrons using CHee and CHee+. The MCNP Manual does not make it clear that an excessive increase in ESTEP, as in CHee + simulations, should be avoided. Using it, for the best case (0.5 keV electrons) CHee and CHee + showed similar differences from RV. Such fact, associated with the high computational time and the possibility of generating instabilities in the CH algorithm seems to discourage this practice of excessively increasing ESTEP value.

DPK results for beta emitter radionuclides showed lower variations among codes than DPK results obtained for the monoenergetic electrons. Wu and coworkers found similar results using MCNP5 and FLUKA (Wu et al., 2012). Each calculated point in the DPK curve represents the ratio of dose in a sphere shell relative to the dose in the entire sphere of radius R_0. For monoenergetic sources all curves showed the same pattern. The most of the energy is deposited within the spherical region corresponding to approximately 60% of its radius (CSDA range) and doses in the shells beyond this point decrease rapidly. However, in realistic cases, i.e., when radionuclides with their energy emission spectra are simulated, DPK results present smoother curves along the R_0 radius, without the well-defined peak of energy deposition. MC codes present small differences in these cases and consistent DPK results were observed. Thus, studies related target radionuclide therapy and beta-emitting seeds brachytherapy using different MC codes and radionuclides studied here should present comparable results. It is very important due to the difficulty in obtaining experimental results.

As far as we know, no study has presented TOPAS DPK values for monoenergetic electrons and beta spectra, comparing the results with other codes. TOPAS present results in good agreement with EGSnrc and the other codes evaluated, proven to be reliable for this type of simulations. It should be remembered that, in this study, the default configuration for electron transport was used in simulations with the TOPAS code. Over the past five years GEANT-DNA electron transport was greatly improved (Kyriakou et al., 2015, 2016) and these

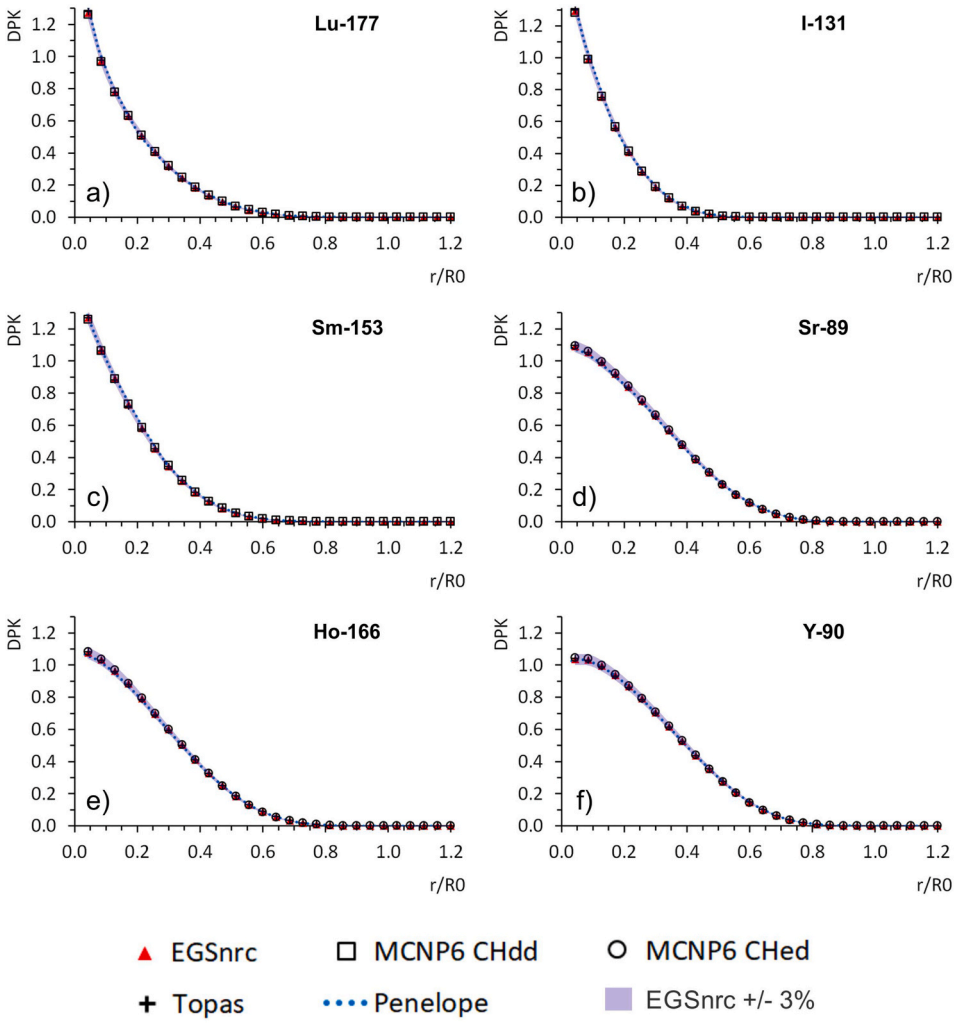

Fig. 4. DPK curves obtained with different codes for 6 radionuclides: a) Lu-177, b) I-131, c) Sm-153, d) Sr-89, e) Ho-166 and f) Y-90.

developments, in terms of physics constructors, can be applied for tuning TOPAS simulations. In this way, future assessments can be made to investigate if some of these new options, in terms of physics constructors, can further improve the performance of this code, especially for 0.05 MeV and 3.0 MeV.

4. Conclusions

Experimental validations for electron energy deposition are very difficult, especially for the region near to the source, small volumes and low energy electrons. Benchmarking, such as the DPK comparison, remains a good option to evaluate the electron energy transport of different Monte Carlo codes.

In this study, the results obtained in the simulations using monoenergetic electron sources ranging from 0.05 up to 3.0 MeV, demonstrated that EGSnrc and PENELOPE MC codes had good agreement in the 0.9 R_0 range. The 0.05 MeV–3.0 MeV energy range cover the majority of radionuclides energy spectra in nuclear medicine. TOPAS also presented results compatible with EGSnrc and PENELOPE, especially for electrons with energies of 0.05 MeV–1.0 MeV. For 3.0 MeV, only the last shell in 0.9 R_0 range presented the differences higher than 10%; this can be attributed to the track structure nature of the electron transport used in TOPAS simulations. This fact is of lesser concern, since more than 90% of electron energy was already deposited before this shell and beta emissions in 3.0 MeV range are considerably rare.

The MCNP6 code showed results compatible with the other codes for 0.05 MeV, using the SE transport algorithm. The same was observed for energy sources of 0.5 MeV, 1.0 MeV and 3.0 MeV when using condensed-history routines (CHee to 0.5 MeV and CHed for both 1.0 and 3.0 MeV). The choice of the electron transport algorithm was found important to obtain the best correlation with EGSnrc DPK values when simulating monoenergetic electrons. DPK values for 0.1 MeV monoenergetic electrons, calculated using MCNP6, found deviating higher than ±5% from RV despite the attempts made to tune electron transport algorithms and physic parameters. Thus, further approaches regarding tuning of MCNP6 electron transport parameters for 0.1 MeV monoenergetic electrons would be desirable in the future.

All MC codes studied in this work could provide DPK values with differences less than ±3% in the r_{E90} range, for all simulated beta-emitting radionuclides (Lu-177, I-131, Sm-153, Sr-89, Ho-166 and Y-90). DPK results obtained with MCNP6 CH routines show better correlation with other codes for low energy beta-emitters (CHdd) as well as to high energy beta-emitters (CHed).

CRediT authorship contribution statement

Bruno Melo Mendes: Conceptualization, Methodology, Software, Formal analysis, Writing - original draft. **Paula Cristina Guimarães Antunes:** Methodology, Software, Investigation. **Isabela Soares Lopes Branco:** Methodology, Software, Investigation. **Eduardo do Nascimento:** Methodology, Software, Investigation. **Baljeet Seniwal:** Methodology, Software, Investigation, Writing - original draft. **Telma**

Cristina Ferreira Fonseca: Supervision. **Helio Yoriyaz:** Conceptualization, Methodology, Software, Formal analysis, Writing - original draft, Supervision.

Declaration of competing interest

The authors declare that they have no known competing financial interests or personal relationships that could have appeared to influence the work reported in this paper.

Acknowledgements

We would like to thank Dr. Ernesto Mainegra-Hing from National Research Council, Canada for helpful discussions on fluence calculations using EGSnrc. The following Brazilian institutions supported this research project: Fundação de Amparo à Pesquisa de Minas Gerais (FAPEMIG) - APQ-00083-18 and APQ-03582-18, Fundação de Amparo à Pesquisa do Estado de São Paulo (FAPESP) and Conselho Nacional de Desenvolvimento Científico e Tecnológico (CNPq) - 450493/2019-9 and 168933/2018-7.

Appendix A. Supplementary data

Supplementary data to this article can be found online at https://doi.org/10.1016/j.radphyschem.2020.109327.

References

Allison, J., et al., 2016. Recent developments in GEANT4. Nucl. Instruments Methods Phys. Res. Sect. A Accel. Spectrometers, Detect. Assoc. Equip. 835, 186–225. https://doi.org/10.1016/j.nima.2016.06.125.

Anjomrouz, M., Bakht, M.K., Praseodymium, C.Á., 2016. Feasibility study of FLUKA Monte Carlo simulation for a beta- emitting brachytherapy source : dosimetric parameters of 142 Pr glass seed. J. Radioanal. Nucl. Chem. 309, 947–953. https://doi.org/10.1007/s10967-016-4744-2.

Antoni, R., Bourgois, L., 2017. Evaluation of the new electron-transport algorithm in MCNP6.1 for the simulation of dose point kernel in water. Nucl. Instruments Methods Phys. Res. Sect. B Beam Interact. with Mater. Atoms 412, 102–108. https://doi.org/10.1016/j.nimb.2017.09.026.

Baró, J., Sempau, J., Ferntidez-Varea, J.M., Salvat, F., 1995. PENELOPE: an Algorithm for Monte Carlo Simulation of the Penetration and Energy Loss of Electrons and Positrons in Matter, vol. 100, pp. 31–46.

Botta, F., Mairani, A., Battistoni, G., Cremonesi, M., Di Dia, A., Fassò, A., Ferrari, A., Ferrari, M., Paganelli, G., Pedroli, G., Valente, M., 2011. Calculation of electron and isotopes dose point kernels with FLUKA Monte Carlo code for dosimetry in nuclear medicine therapy. Med. Phys. 38, 3944–3954. https://doi.org/10.1118/1.3586038.

Bousis, C., Emfietzoglou, D., Hadjidoukas, P., Nikjoo, H., 2008. A Monte Carlo study of absorbed dose distributions in both the vapor and liquid phases of water by intermediate energy electrons based on different condensed-history transport schemes. Phys. Med. Biol. 53, 3739–3761. https://doi.org/10.1088/0031-9155/53/14/003.

Bousis, C., Emfietzoglou, D., Hadjidoukas, P., Nikjoo, H., 2010. Monte Carlo single-cell dosimetry of Auger-electron emitting radionuclides. Phys. Med. Biol. 55, 2555–2572. https://doi.org/10.1088/0031-9155/55/9/009.

Calandrino, R., Del Vecchio, A., Todde, S., Fazio, F., 2007. Measurement and control of the air contamination generated in a medical cyclotron facility for PET radiopharmaceuticals. Health Phys. 92 https://doi.org/10.1097/01.HP.0000253941.56400.76.

Champion, C., Incerti, S., Perrot, Y., Delorme, R., Bordage, M.C., Bardiès, M., Mascialino, B., Tran, H.N., Ivanchenko, V., Bernal, M., Francis, Z., Groetz, J.E., Fromm, M., Campos, L., 2014. Dose point kernels in liquid water: an intra-comparison between GEANT4-DNA and a variety of Monte Carlo codes. Appl. Radiat. Isot. 83, 137–141. https://doi.org/10.1016/j.apradiso.2013.01.037.

Fonseca, T.C.F., Antunes, P.C.G., Belo, M.C.L., Bastos, F., Campos, T.P., Geraldo, J.M., Mendes, A.M., Mendes, B.M., Paixão, L., Santana, P.C., Seniwal, B., Squair, P.L., Yoriyaz, H., 2020. MCMEG: intercomparison exercise on prostate radiotherapy dose assessment. Radiat. Phys. Chem. 167, 108295. https://doi.org/10.1016/j.radphyschem.2019.04.045.

Goorley, J.T., James, M.R., Booth, T.E., Brown, F.B., Bull, J.S., Cox, L.J., Durkee, J.W., Elson, J.S., Fensin, M.L., Forster, R.A., Hendricks, J.S., Hughes, H.G., Johns, R.C., Kiedrowski, B.C., Mashnik, S.G., 2013. MCNP6 user's manual, version 1.0, LA-CP-13-00634. Los Alamos Natl. Lab. pp. 1–765.

Gudkov, S.V., Shilyagina, N.Y., Vodeneev, V.A., Zvyagin, A.V., 2015. Targeted radionuclide therapy of human tumors. Int. J. Mol. Sci. 17, 1–19. https://doi.org/10.3390/ijms17010033.

Hadadi, A., Sadeghi, M., Sardari, D., Khanchi, A., Shirazi, A., 2013. Monte Carlo characterization of biocompatible beta-emitting 90Y glass seed incorporated with the radionuclide 153Sm as a SPECT marker for brachytherapy applications. J. Appl. Clin. Med. Phys. 14, 90–103. https://doi.org/10.1120/jacmp.v14i5.4302.

Hindorf, C., Emfietzoglou, D., Lindén, O., Kostarelos, K., Strand, S.E., 2005. Internal microdosimetry for single cells in radioimmunotherapy of B-cell lymphoma. Cancer Biother. Radiopharm 20, 224–230. https://doi.org/10.1089/cbr.2005.20.224.

Hindorf, C., Emfietzoglou, D., Lindén, O., Bousis, C., Fotopoulos, A., Kostarelos, K., Flux, G.D., 2007. Single-cell dosimetry for radioimmunotherapy of B-cell lymphoma patients with special reference to leukemic spread. Cancer Biother. Radiopharm. 22, 357–366. https://doi.org/10.1089/cbr.2007.347.

Hosseini, S.H., Enferadi, M., Sadeghi, M., 2013. Dosimetric aspects of 166Ho brachytherapy biodegradable glass seed. Appl. Radiat. Isot. 73, 109–115. https://doi.org/10.1016/j.apradiso.2012.12.002.

Hughes, G., 2014. Recent developments in low-energy electron/photon transport for MCNP6. Prog. Nucl. Sci. Technol. 4, 454–458. https://doi.org/10.15669/pnst.4.454.

ICRP, 2007. The 2007 recommendations of the international commission on radiological protection. Ann. ICRP 37, 1–332. https://doi.org/10.1016/j.icrp.2007.11.001.

Jeon, J., 2019. Review of therapeutic applications of radiolabeled functional nanomaterials. Int. J. Mol. Sci. 20 https://doi.org/10.3390/ijms20092323.

Jung, J.W., Reece, W.D., 2008. Dosimetric characterization of 142Pr glass seeds for brachytherapy. Appl. Radiat. Isot. 66, 441–449. https://doi.org/10.1016/j.apradiso.2007.11.008.

Kawrakow, I., Rogers, D.W.O., 2013. EGSnrc: the EGSnrc code System : Monte Carlo simulation of electron and photon transport [WWW Document]. Man. - Guid. URL. https://nrc-cnrc.github.io/EGSnrc/doc/pirs701-egsnrc.pdf.

Khorshidi, A., Ahmadinejad, M., Hosseini, S.H., 2015. Evaluation of a proposed biodegradable 188Re source for brachytherapy application: a review of dosimetric parameters. Med. (United States) 94, 1–7. https://doi.org/10.1097/MD.0000000000001098.

Kyriakou, I., Incerti, S., Francis, Z., 2015. Technical note: improvements in geant 4 energy-loss model and the effect on low-energy electron transport in liquid water. Med. Phys. 42, 3870–3876. https://doi.org/10.1118/1.4921613.

Kyriakou, I., Šefl, M., Nourry, V., Incerti, S., 2016. The impact of new Geant4-DNA cross section models on electron track structure simulations in liquid water. J. Appl. Phys. 119 https://doi.org/10.1063/1.4950808.

Kyriakou, I., Ivanchenko, V., Sakata, D., Bordage, M.C., Guatelli, S., Incerti, S., Emfietzoglou, D., 2019. Influence of track structure and condensed history physics models of Geant4 to nanoscale electron transport in liquid water. Phys. Medica 58, 149–154. https://doi.org/10.1016/j.ejmp.2019.01.001.

Li, T., Ao, E.C.I., Lambert, B., Brans, B., Vandenberghe, S., Mok, G.S.P., 2017. Quantitative imaging for targeted radionuclide therapy dosimetry - technical review. Theranostics 7, 4551–4565. https://doi.org/10.7150/thno.19782.

Maigne, L., Perrot, Y., Schaart, D.R., Donnarieix, D., Breton, V., 2011. Comparison of GATE/GEANT4 with EGSnrc and MCNP for electron dose calculations at energies between 15 keV and 20 MeV. Phys. Med. Biol. 56, 811–827. https://doi.org/10.1088/0031-9155/56/3/017.

Passos, T., Campos, R. De, Batista, L., Trindade, B., Mizrahy, E., 2016. Dosimetric intercomparison of permanent Ho-166 seed ' s implants and HDR Ir-192 brachytherapy in. Reports Pract. Oncol. Radiother. 21, 240–249. https://doi.org/10.1016/j.rpor.2015.11.007.

Pelowitz, D.B., 2011. Mcnpx user's manual - version 2.7.0. https://www.researchgate.net/publication/263008961_MCNPX_User's_Manual_Version_270.

Perl, J., Shin, J., Schümann, J., Faddegon, B., Paganetti, H., 2012. TOPAS: an innovative proton Monte Carlo platform for research and clinical applications. Med. Phys. 39, 6818–6837. https://doi.org/10.1118/1.4758060.

Poškus, A., 2016. Evaluation of computational models and cross sections used by MCNP6 for simulation of electron backscattering. Nucl. Instruments Methods Phys. Res. Sect. B Beam Interact. with Mater. Atoms 368, 15–27. https://doi.org/10.1016/j.nimb.2015.11.027.

RADAR, 2002. Radar - the decay data [WWW Document]. Resour. Radiat. Dose Assess. URL. https://doseinfo-radar.com/RADARDecay.html (accessed 11.26.19).

Reynaert, N., Palmans, H., Thierens, H., Jeraj, R., 2002. Parameter dependence of the MCNP electron transport in determining dose distributions. Med. Phys. 29, 2446–2454. https://doi.org/10.1118/1.1508798.

Roberto, W.S., Pereira, M.M., Campos, T.P.R. de, 2003a. Analysis of bioactive glasses obtained by sol-gel processing for radioactive implants. Mater. Res. 6, 123–127. https://doi.org/10.1590/s1516-14392003000200003.

Roberto, W.S., Pereira, M.M., Campos, T.P.R., 2003b. Structure and dosimetric analysis of biodegradable glasses for prostate cancer treatment. Artif. Organs 27, 432–436. https://doi.org/10.1046/j.1525-1594.2003.07253.x.

Salvat, F., Fernández-Varea, J.M., 2015. Penelope – a code system for Monte Carlo simulation of electron and photon transport organisation for economic CO-operation and development [WWW Document]. PENELOPE, a code Syst. Monte Carlo Simul. electron Phot. Transp. URL. https://www.oecd-nea.org/science/docs/2015/nsc-doc2015-3.pdf.

Sapienza, T.S., Willegaignon, J., 2019. Radionuclide therapy : current status and prospects for internal dosimetry in individualized therapeutic planning. Clinics 74, 1–8. https://doi.org/10.6061/clinics/2019/e835.

Sato, T., Niita, K., Matsuda, N., Hashimoto, S., Iwamoto, Y., Furuta, T., Noda, S., Ogawa, T., Iwase, H., Nakashima, H., Fukahori, T., Okumura, K., Kai, T., Chiba, S., Sihver, L., 2015. Overview of particle and heavy ion transport code system PHITS. Ann. Nucl. Energy 82, 110–115. https://doi.org/10.1016/j.anucene.2014.08.023.

Sempau, J., Badal, A., Brualla, L., 2011. A PENELOPE-based system for the automated Monte Carlo simulation of clinacs and voxelized geometries-application to far-from-axis fields. Med. Phys. 38, 5887–5895. https://doi.org/10.1118/1.3643029.

Seniwal, B., Fonseca, T.C.F., Singh, R., 2019. Monte-Carlo modelling for evaluation of two different calculation algorithms. Brazilian J. Radiat. Sci. 7, 1–14. https://doi.org/10.15392/bjrs.v7i1.792.

Seniwal, B., Bernal, M.A., Fonseca, T.C.F., 2020a. Microdosimetric calculations for radionuclides emitting β and α particles and Auger electrons. Appl. Radiat. Isot. 166, 109302. https://doi.org/10.1016/j.apradiso.2020.109302.

Seniwal, B., Bhatt, C.P., Fonseca, T.C.F., 2020b. Comparison of dosimetric accuracy of acuros XB and analytical anisotropic algorithm against Monte Carlo technique. Biomed. Phys. Eng. Express 6, 15035. https://doi.org/10.1088/2057-1976/ab6e1b.

Syme, A.M., Kirkby, C., Riauka, T.A., Fallone, B.G., McQuarrie, S.A., 2004. Monte Carlo investigation of single cell beta dosimetry for intraperitoneal radionuclide therapy. Phys. Med. Biol. 49, 1959–1972. https://doi.org/10.1088/0031-9155/49/10/009.

TOPAS, M.C., 2016. TOPAS modular physics lists [WWW Document]. TOPAS MC Inc Revis. f18b1167. URL. https://topas.readthedocs.io/en/latest/parameters/physics/modular.html (accessed 1.9.20).

Wang, J.T.W., Klippstein, R., Martincic, M., Pach, E., Feldman, R., Šefl, M., Michel, Y., Asker, D., Sosabowski, J.K., Kalbac, M., Da Ros, T., Ménard-Moyon, C., Bianco, A., Kyriakou, I., Emfietzoglou, D., Saccavini, J.C., Ballesteros, B., Al-Jamal, K.T., Tobias, G., 2020a. Neutron activated 153Sm sealed in carbon nanocapsules for in vivo imaging and tumor radiotherapy. ACS Nano 14, 129–141. https://doi.org/10.1021/acsnano.9b04898.

Wang, J.T.W., Spinato, C., Klippstein, R., Costa, P.M., Martincic, M., Pach, E., Ruiz de Garibay, A.P., Ménard-Moyon, C., Feldman, R., Michel, Y., Šefl, M., Kyriakou, I., Emfietzoglou, D., Saccavini, J.C., Ballesteros, B., Tobias, G., Bianco, A., Al-Jamal, K. T., 2020b. Neutron-irradiated antibody-functionalised carbon nanocapsules for targeted cancer radiotherapy. Carbon N. Y. 162, 410–422. https://doi.org/10.1016/j.carbon.2020.02.060.

Wheat, J.M., Currie, G.M., Davidson, R., Kiat, H., 2011. Radionuclide therapy. Radiogr 58, 53–59.

Wu, J., Liu, Y.L., Chang, S.J., Chao, M.M., Tsai, S.Y., Huang, D.E., 2012. Dose point kernel simulation for monoenergetic electrons and radionuclides using monte carlo techniques. Radiat. Prot. Dosimetry 152, 119–124. https://doi.org/10.1093/rpd/ncs204.

X-5 Monte Carlo Team, 2008. In: Girard, M., Sheila (Eds.), MCNP — A General Monte Carlo N-Particle Transport Code, Version 5. Volume I: Overview and Theory. Los Alamos National Laboratory, pp. 1–416.